Hindawi
International Journal of Aerospace Engineering
Volume 2020, Article ID 7025374, 12 pages
https://doi.org/10.1155/2020/7025374

Research Article

Development of Real-Time Maneuver Library Generation Technique for Implementing Tactical Maneuvers of Fixed-Wing Aircraft

Do hyeon Lee[1], **Chang-Joo Kim**[2], **Man Jung Heo**[1], **Joo Wan Hwang**[1], **Hee Gyeong Lyu**[1] and **Jun Yeop Lee**[1]

[1]*Core Technology Development Team, Hanwha Defense, Seongnam-si 13488, Republic of Korea*
[2]*Aerospace Information Engineering, Konkuk University, Seoul 05029, Republic of Korea*

Correspondence should be addressed to Chang-Joo Kim; cjkim@konkuk.ac.kr

Received 16 August 2019; Revised 24 November 2019; Accepted 12 December 2019; Published 16 January 2020

Academic Editor: Rosario Pecora

This study develops the real-time maneuver library generation technique for performing aggressive maneuvers of fixed-wing aircraft. Firstly, the general maneuver libraries are defined, and then 7^{th}-order polynomials are used to create the maneuver libraries. The attitude command attitude hold (ACAH) system, the rate command rate hold (RCRH) system, and the speed command speed hold (SCSH) system using the proportional-integral-derivative (PID) control technique are designed to minimize the complexity of the flight control system (FCS) and to reduce the weight and volume of the payload. Moreover, the FCS is used for implementing tactical maneuvers. Finally, flight simulations are implemented for the longitudinal loop and Immelmann-turn maneuvers to check the usefulness of the proposed maneuver library generation technique. This study can affect the development of flight techniques for aircraft tactical maneuvers and the modification of air force operational manuals.

1. Introduction

The flight performance of manned or unmanned aircraft has to be maximized to perform the entire mission in dynamically changing environments such as battlefields. Most researchers have developed the flight path generation techniques by using a numerical optimization algorithm (NOA) to maximize the flight performance and to guarantee the survivability of aircraft [1]. However, the NOA has the two disadvantages. First, the NOA cannot guarantee the real-time flight path generation. The constraints and boundary conditions are defined when the flight path is generated. The increment of the number of constraints and boundary conditions reduces the calculation speed of NOA. To overcome this disadvantage, the parallel processing method is applied to the NOA. However, state-of-the-art processors using parallel processing methods raise the weight and volume of the payload. Also, the electric power consumption is increased. So, small aircraft cannot use the state-of-the-art processor. Second, NOA does not guarantee existence of solution satisfying the constraints and boundary conditions. This is the most critical disadvantage of NOA. So the NOA cannot be used in battlefields because the environment of battlefields rapidly changes. Finally, flight path generation using NOA is possible when designers know the physical characteristics and information of the target maneuvers. It means that the NOA cannot deal with unexpected situations. Therefore, a new algorithm has to be developed to perform the mission with tactical maneuvers. The main contributions of this paper are the development of real-time maneuver library generation techniques to overcome easily the disadvantages of NOA. Furthermore, the FCS is constructed by PID control technique to minimize the complexity of FCS and to reduce the weight and volume of the payload. The FCS uses the maneuver libraries to address simply the various types of aggressive maneuvers according to situations.

The existing techniques to perform the aggressive maneuvers have been examined to define the data type of maneuver libraries and to generalize the maneuver libraries. The existing researches associated with an aggressive maneuver are as follows. Ure et al. [2, 3] studied on the flight path generation to implement the missions for the unmanned combat aerial vehicle (UCAV). They also researched the control framework for aggressive maneuvers, using a sliding mode controller. Koo et al. [4] studied the conditions for flight maneuver transition and the diversity of flight paths according to combinations of maneuver. Wang et al. [5] proposed the flight maneuver identification method from flight test data. Moreover, they stored the data as libraries. Sankalp et al. [6] researched the maneuver library generation to ensure the stability of a rotorcraft in a given environment. However, they did not mention the definition of maneuver libraries. Bry et al. [7] checked the build of the flight control framework for tactical maneuvers of fixed-wing and quadrotor aircraft. Barry et al. [8] studied the autonomous obstacle avoidance algorithm for agile flight. Brian [9] researched the aerobatic maneuvers for fixed-wing aircraft by using a classical controller, whereas Willem [10] studied the aerobatic maneuvers for fixed-wing aircraft by using a nonlinear control technique. Edwards [11] and Tatsch [12] described the procedures of aggressive maneuvers for propeller-driven aircraft. The researches of Edward and Tatsch indicate that the aggressive maneuvers require the transition of flight controllers and maneuvers. van der Plas and Visser [13] optimized the flight path after dividing the flight path into several segments. Thomson and Bradley [14] researched the flight path generation method using polynomials, and Lee et al. [15, 16] studied the flight path generation using a polynomial and tracking control technique. The existing studies indicate that (1) the aggressive maneuvers have to be divided into several segments. Also, (2) a new concept of trajectories is required, which is not the flight paths. Finally, (3) the flight controllers have to be transitioned to perform tactical maneuvers and must be simple. Thus, these concepts have to be converged into the development of a real-time maneuver library generation technique and multi-FCS to perform the tactical maneuvers.

This study tries to show the usefulness of the suggested method by performing tactical maneuvers with the combination of general maneuver libraries and the transition of FCS. Thus, the general maneuver libraries and the modal inputs are defined. In particular, the modal inputs are used to distinguish the general maneuver libraries, and they are the key parameters for generating maneuver libraries. Then, the general maneuver libraries are established by 7^{th}-order polynomial. The attitude command attitude hold (ACAH) system, the rate command rate hold (RCRH) system, and the speed command and speed hold (SCSH) system are designed as FCS to perform the tactical maneuvers through the combination of maneuver libraries. Finally, flight simulations for the longitudinal loop and the Immelmann-turn maneuvers are performed to verify the possibility of realization of the proposed method.

The rest of this paper is organized as follows. Section 2 introduces general maneuver libraries, and Section 3 describes the creation of maneuver libraries based on a 7^{th}-order polynomial. Section 4 deals with the design of the FCS. Section 5 analyzes the flight simulation of tactical maneuvers. Section 6 is the conclusion of this research.

2. General Maneuver Library

Figure 1 indicates a procedure of the air-to-surface mission. In (2), the terrain-masking maneuvers are implemented from the front line. In (3) and (4), the target may be successfully hit by performing the various tactical maneuvers to avoid the enemy radars and surface-to-air missiles. In (5), the terrain-masking maneuvers are implemented again to exit the mission area. Therefore, aggressive maneuvers are needed in the areas of (2)–(5) [17]. The maneuver properties of (1)–(5) are described in Table 1.

The maneuver libraries have to be generalized as in Table 2 to perform the tactical maneuvers. In particular, each maneuver library has several modal inputs and the FCS. The modal inputs are the most basic state variables to distinguish the maneuver libraries. Thus, the trajectories of modal inputs have to be created, which are the new concept of trajectories in this research. The new concept of trajectories is defined as maneuver libraries. So generating maneuver libraries is the same as creating the trajectory of modal inputs. The FCS must track the trajectory of modal inputs to perform the aggressive maneuvers. Thus, the modal inputs define the aggressiveness and precision of tactical maneuvers, and they are used as a reference signal for FCS. The detailed information is described in Ref. [18].

The angular rates, attitude angles, rate of altitude, angle of attack, and flight velocity have to be measured to use the trajectory of modal inputs as reference signals for FCS. The angular rates $[p\,q\,r]^T$ and the attitude angles $[\phi \quad \theta \quad \psi]^T$ can be measured by a gyro sensor. Also, the angle of attack α, rate of altitude $\dot{h}$, and flight velocity V_T are measured by pitot tube. However, the angular accelerations cannot be measured by a gyro sensor. Most gyro sensors do not provide the value of angular accelerations. Thus, the angular accelerations are not used as modal inputs. This research is assuming that the wind disturbances and the sensor noise do not exist while measuring the variables such as angular rates, attitude angles, rate of altitude, angle of attack, and flight velocity. Thus, the FCS does not consider the noise cancel technique.

3. Maneuver Library Generation

This research tries to generate maneuver libraries by using the 7^{th}-order polynomials. The reason why a polynomial is employed is that a polynomial can overcome the two disadvantages of NOA [15]. The disadvantages of NOA are already described in Section 1. Several solutions to overcome the disadvantages of NOA have been suggested. However, complete solutions have not yet been developed. This study utilizes the polynomial to generate the maneuver libraries. The polynomial can guarantee the real-time maneuver library generation while satisfying the required boundary conditions or constraints.

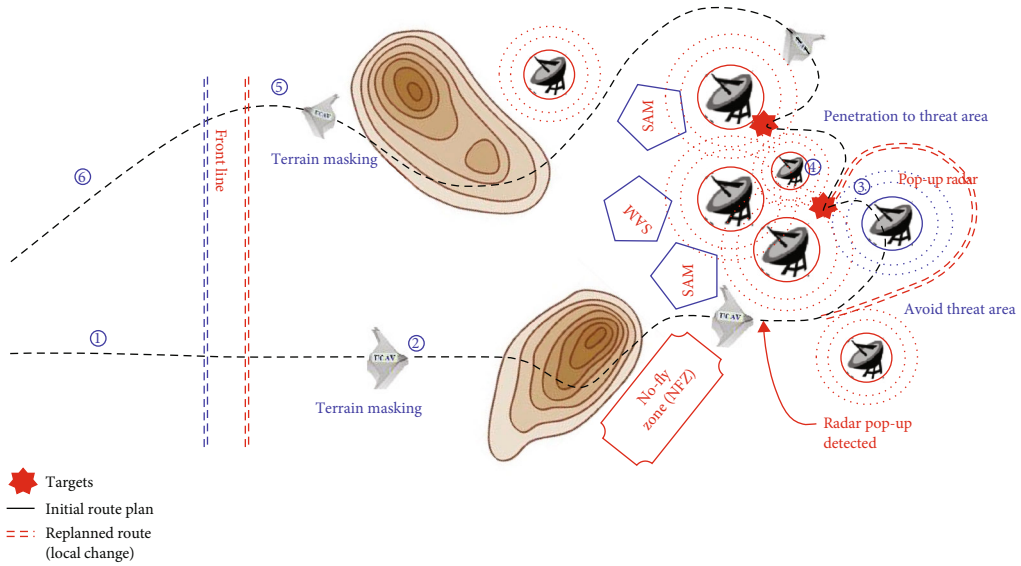

Figure 1: Procedure of the air-to-surface mission [18].

Table 1: Maneuver properties of the air-to-surface mission [18].

	Mission phase	Maneuver property	Element category of mission task
(1)	Take-off, operations in the safe zone	Nonaggressive/nonprecision tasks	Category B
(2)	Ingress terrain following in the enemy zone	Aggressive/precision tasks	Category A
(3)	Ingress to the threat zone/approach to target/target acquisition and missile engagement	Aggressive/precision tasks	Category A
(4)	Egress maneuver from the highly threatened zone	Aggressive/nonprecision tasks	Category D
(5)	Egress terrain following in the enemy zone	Aggressive/precision tasks	Category A
(6)	Landing, operations in the safe zone	Nonaggressive/nonprecision tasks	Category B

Table 2: General maneuver libraries, modal inputs, and FCS for each maneuver [2, 18].

	Maneuver library	State constraints	Modal input	Controller
q_0	Level flight	$\dot{h} = 0, \left(\dot{\phi}, \dot{\theta}, \dot{\psi}\right) = 0$	V_T, α	(i) SCSH system (ii) ACAH system
q_1	Climb/descent	$\left(\dot{\phi}, \dot{\psi}\right) = 0$	$V_T, \dot{h}$	(i) SCSH system (ii) ACAH system
q_2	Roll	$\left(\dot{\theta}, \dot{\psi}\right) = 0$	$V_T, \dot{\phi}$	(i) SCSH system (ii) RCRH system
q_3	Longitudinal loop	$\left(\dot{\phi}, \dot{\psi}\right) = 0$	$V_T, \dot{\theta}, r_{\text{loop}}$	(i) SCSH system (ii) RCRH system
q_4	Lateral loop	$\dot{h} = 0, \left(\dot{\phi}, \dot{\theta}\right) = 0$	$V_T, \dot{\psi}, r_{\text{loop}}$	(i) SCSH system (ii) RCRH system
⋮	⋮	⋮	⋮	⋮

Thomson and Bradley [14] had suggested the acceleration model to generate the trajectory, which is used for generating the helicopter flight path. In this study, the acceleration model suggested by Douglas Thomson and Bradley and 7$^{\text{th}}$-order polynomials are used for generating maneuver libraries.

As shown in Figure 2, the acceleration model to generate the maneuver libraries is divided into 5 phases such as the entry, maximum acceleration, transition, minimum acceleration, and exit phases to reflect the required aggressiveness of the maneuver. In particular, the durations of the entry and exit phases mean the aggressiveness of the maneuver. The trajectory of each phase can be generated by a 7$^{\text{th}}$-order polynomial.

3.1. Entry Phase. The aggressiveness for tactical maneuvers is associated with the time interval Δt_1 and $\dot{\omega}_{\max}$. Here, Δt_1 is the time interval for the entry phase, and $\dot{\omega}_{\max}$ is the

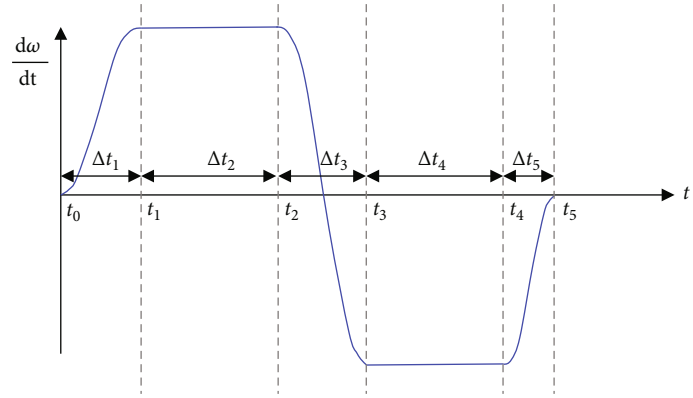

Figure 2: Modeling the acceleration for trajectory [14, 18].

maximum acceleration for the maximum acceleration phase and minimum acceleration phase. If Δt_1 is increased, the more $\dot{\omega}_{\max}$ is decreased. Also, if Δt_1 is decreased, $\dot{\omega}_{\max}$ is increased. So, $\dot{\omega}_{\max}$ should be numerically calculated to satisfy the boundary conditions when Δt_1 has been determined [16]. $\dot{\omega}_{\max_0}$ is the initial value for calculating maximum acceleration, which can be defined by Equation (1). Then, $\dot{\omega}_{\max}$ will be calculated by the Newton-Raphson numerical method to satisfy the boundary conditions [16]:

$$\begin{aligned} \dot{\omega}_{\max_0} &= \frac{\theta_f - \theta_0}{\Delta t_1{}^2}, \\ \Delta t_1 &= t_1 - t_0, \end{aligned} \tag{1}$$

where θ_0 and θ_f indicate the initial and final conditions, respectively. To easily generate the trajectories, $\theta(t)$ for the entry phase, the nondimension time variable τ is used instead of the real-time variable t as shown in

$$\tau = \frac{t - t_0}{t_1 - t_0}, \quad 0 \le \tau \le 1. \tag{2}$$

The trajectory of $\overline{\theta}(\tau)$, $\bar{\omega}(\tau)$, and $\dot{\bar{\omega}}(\tau)$ can be defined as shown in

$$\begin{aligned} \overline{\theta}(\tau) &= a + b\tau + c\tau^2 + d\tau^3 + e\tau^4 + p\tau^5 + q\tau^6 + r\tau^7, \\ \omega(t) &= \frac{d\overline{\theta}}{dt} = \frac{d\overline{\theta}}{d\tau}\frac{d\tau}{dt} = \frac{1}{\Delta t_1}\frac{d\overline{\theta}}{d\tau} = \frac{1}{\Delta t_1}\dot{\overline{\theta}}(\tau), \\ \bar{\omega}(\tau) &= \dot{\overline{\theta}}(\tau) = \omega(t) \cdot (\Delta t_1), \\ \dot{\bar{\omega}}(\tau) &= \ddot{\overline{\theta}}(\tau) = \dot{\omega}(t) \cdot (\Delta t_1)^2. \end{aligned} \tag{3}$$

The 7th-order polynomial has 8 coefficients, so the 4 initial conditions and the 4 final conditions are necessary to generate the $\overline{\theta}(\tau)$. These 8 conditions are used as boundary conditions for generating $\overline{\theta}(\tau)$. Thus, the boundary conditions to generate the trajectory $\overline{\theta}(\tau)$ are defined as shown in

$$\begin{aligned} \begin{bmatrix} \overline{\theta}(0) \\ \bar{\omega}(0) \\ \dot{\bar{\omega}}(0) \\ \ddot{\bar{\omega}}(0) \end{bmatrix} &= \begin{bmatrix} \theta(t_0) \\ \omega(t_0) \cdot (\Delta t_1) \\ \dot{\omega}(t_0) \cdot (\Delta t_1)^2 \\ 0 \end{bmatrix}, \\ \begin{bmatrix} \dot{\bar{\omega}}(1) \\ \ddot{\bar{\omega}}(1) \\ \dddot{\bar{\omega}}(1) \\ \bar{\omega}^{(4)}(1) \end{bmatrix} &= \begin{bmatrix} \dot{\omega}_{\max}(t_1) \cdot (\Delta t_1)^2 \\ 0 \\ 0 \\ 0 \end{bmatrix}. \end{aligned} \tag{4}$$

Here, "0" means the initial time and "1" means the final time in the nondimensional time interval. The maximum acceleration at "1" for the entry phase is the key variable because the maximum acceleration is used to define the final conditions constructed by derivatives of equal to or higher than the second order for $\overline{\theta}(\tau)$. The final conditions are used to provide the smoothness of the created trajectory.

From Equation (4), the four coefficients a, b, c, and d are simply calculated by initial conditions, and the other coefficients e, f, g, and h are computed by final conditions as shown in Equation (5). Furthermore, e, f, g, and h can be easily determined by Equation (6).

$$\begin{aligned} a &= \overline{\theta}(0), \\ b &= \bar{\omega}(0), \\ c &= \frac{1}{2}\dot{\bar{\omega}}(0), \\ d &= 0.0, \\ \dot{\bar{\omega}}(1) &= 2c + 6d + 12e + 20f + 30g + 42h, \\ \ddot{\bar{\omega}}(1) &= 6d + 24e + 60f + 120g + 210h, \\ \dddot{\bar{\omega}}(1) &= 24e + 120f + 360g + 840h, \\ \bar{\omega}^{(4)}(1) &= 120f + 720g + 2520h, \end{aligned} \tag{5}$$

$$\begin{bmatrix} 12 & 20 & 30 & 42 \\ 24 & 60 & 120 & 210 \\ 24 & 120 & 360 & 840 \\ 0 & 120 & 720 & 2520 \end{bmatrix} \begin{bmatrix} e \\ f \\ g \\ h \end{bmatrix} = \begin{bmatrix} \dot{\bar{\omega}}(1) - (2c + 6d) \\ \ddot{\bar{\omega}}(1) - 6d \\ \dddot{\bar{\omega}}(1) \\ \bar{\omega}^{(4)}(1) \end{bmatrix}. \tag{6}$$

The trajectory generation of the entry phase is finished by allocating the 8 coefficients to $\overline{\theta}(\tau)$. However, the trajectory $\overline{\theta}(\tau)$ is generated in a nondimensional time domain. Thus, the created trajectories such as $\overline{\theta}(\tau)$, $\bar{\omega}(\tau)$, and $\dot{\bar{\omega}}(\tau)$ should be transformed to the real-time domain from nondimensional time domain as shown in

$$\begin{aligned} \theta(t) &= \overline{\theta}(\tau), \\ \omega(t) &= \frac{\bar{\omega}(\tau)}{\Delta t_1}, \\ \dot{\omega}(t) &= \frac{\dot{\bar{\omega}}(\tau)}{\Delta t_1{}^2}. \end{aligned} \tag{7}$$

3.2. Maximum Acceleration Phase. The procedure of trajectory generation is the same with the entry phase. However, the boundary conditions are different with the entry phase since the maximum acceleration is maintained as constant. So, $\overline{\theta}(\tau)$ can be defined as a 2^{nd}-order polynomial. Thus, the boundary conditions and trajectories of $\overline{\theta}(\tau)$, $\bar{\omega}(\tau)$, and $\dot{\bar{\omega}}(\tau)$ are defined as like Equations (9) and (10).

$$\begin{aligned} \dot{\bar{\omega}}(\tau) &= \text{Const}, \\ \omega(t) &= \frac{\bar{\omega}(\tau)}{\Delta t_1}, \end{aligned} \tag{8}$$

$$\begin{aligned} \begin{bmatrix} \overline{\theta}(0) \\ \bar{\omega}(0) \\ \dot{\bar{\omega}}(0) \\ \ddot{\bar{\omega}}(0) \end{bmatrix} &= \begin{bmatrix} \theta(t_1) \\ \omega(t_1) \cdot (\Delta t_1) \\ \dot{\omega}(t_1) \cdot (\Delta t_1)^2 \\ 0 \end{bmatrix}, \\ \begin{bmatrix} \dot{\bar{\omega}}(1) \\ \ddot{\bar{\omega}}(1) \end{bmatrix} &= \begin{bmatrix} \dot{\omega}(t_2) \cdot (\Delta t_2)^2 \\ 0 \end{bmatrix}, \end{aligned} \tag{9}$$

$$\begin{aligned} \overline{\theta}(\tau) &= \overline{\theta}(0) + \bar{\omega}(0) \cdot (\Delta t_2) \cdot \tau + \frac{1}{2} \dot{\bar{\omega}}(0) \cdot \left(\Delta t_2^2\right) \cdot \tau^2, \\ \bar{\omega}(\tau) &= \bar{\omega}(0) + \dot{\bar{\omega}}(0) \cdot (\Delta t_2) \cdot \tau, \\ \dot{\bar{\omega}}(\tau) &= \dot{\bar{\omega}}(0). \end{aligned} \tag{10}$$

$\theta(t)$, $\omega(t)$, and $\dot{\omega}(t)$ can be defined by Equation (7).

3.3. Transition Phase. The acceleration is transitioned from maximum value to minimum value in this phase. So, the boundary conditions are defined as like the following:

$$\begin{aligned} \dot{\bar{\omega}}(0) &= \dot{\omega}(t_2) \cdot (\Delta t_2)^2, \\ \ddot{\bar{\omega}}(0) &= 0.0, \\ \dddot{\bar{\omega}}(0) &= 0.0, \\ \dot{\bar{\omega}}(1) &= -\dot{\omega}_{\max} \cdot (\Delta t_3)^2, \\ \ddot{\bar{\omega}}(1) &= 0.0, \\ \dddot{\bar{\omega}}(1) &= 0.0. \end{aligned} \tag{11}$$

The six coefficients of the $\dot{\bar{\omega}}(\tau)$ are calculated in the same manner with Equations (5) and (6). However, $\overline{\theta}(\tau)$ and $\bar{\omega}(\tau)$ have to be defined by integrating $\dot{\bar{\omega}}(\tau)$. By utilizing Equation (10), $\overline{\theta}(\tau)$, $\bar{\omega}(\tau)$, and $\dot{\bar{\omega}}(\tau)$ are defined as follows:

$$\begin{aligned} \dot{\bar{\omega}}(\tau) &= a + b\tau + c\tau^2 + d\tau^3 + e\tau^4 + f\tau^5, \\ \bar{\omega}(\tau) &= \bar{\omega}(0) + (\Delta t_3) \int \dot{\bar{\omega}}(\tau) d\tau, \\ \overline{\theta}(\tau) &= \overline{\theta}(0) + \bar{\omega}(0) \cdot (\Delta t_3) \cdot \tau + (\Delta t_3)^2 \iint \dot{\bar{\omega}}(\tau) d\tau d\tau \\ &= a_\theta + b_\theta \tau + c_\theta \tau^2 + d_\theta \tau^3 + e_\theta \tau^4 \\ &\quad + f_\theta \tau^5 + g_\theta \tau^6 + h_\theta \tau^7, \end{aligned} \tag{12}$$

$$\begin{bmatrix} a_\theta \\ b_\theta \\ c_\theta \\ d_\theta \\ e_\theta \\ f_\theta \\ g_\theta \\ h_\theta \end{bmatrix} = \begin{bmatrix} \overline{\theta}(0) \\ \bar{\omega}(0) \cdot (\Delta t_3) \\ \frac{1}{2} a \cdot (\Delta t_3)^2 \\ \frac{1}{6} b \cdot (\Delta t_3)^2 \\ \frac{1}{12} c \cdot (\Delta t_3)^2 \\ \frac{1}{20} d \cdot (\Delta t_3)^2 \\ \frac{1}{30} e \cdot (\Delta t_3)^2 \\ \frac{1}{42} f \cdot (\Delta t_3)^2 \end{bmatrix}. \tag{13}$$

Also, $\theta(t)$, $\omega(t)$, and $\dot{\omega}(t)$ for the transition phase can be defined by Equation (7).

3.4. Minimum Acceleration Phase. This phase maintains the acceleration to minimum value. The boundary conditions and the procedure of defining the polynomials are the same with the maximum acceleration phase.

3.5. Exit Phase. The maneuvers corresponding to each maneuver library are terminated in this phase. So, the

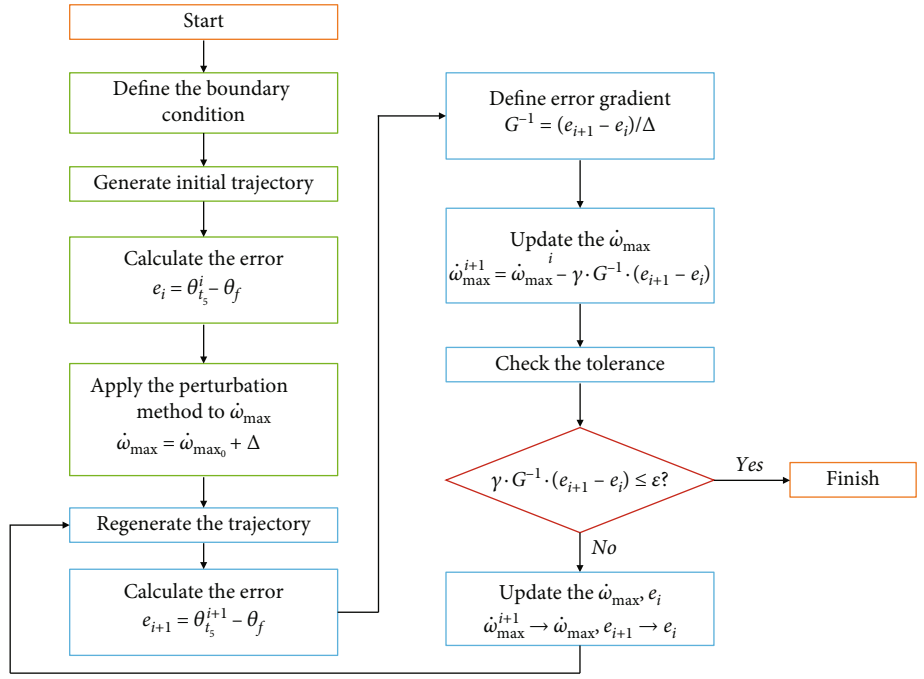

Figure 3: Exact maximum acceleration calculation with the Newton-Raphson method [18].

boundary conditions as coefficients of $\bar{\theta}(\tau)$ are defined as shown in

$$\begin{bmatrix} \bar{\theta}(0) \\ \bar{\omega}(0) \\ \dot{\bar{\omega}}(0) \\ \ddot{\bar{\omega}}(0) \\ \dddot{\bar{\omega}}(0) \end{bmatrix} = \begin{bmatrix} \theta(t_4) \\ \omega(t_4) \cdot (\Delta t_4) \\ \dot{\omega}(t_4) \cdot (\Delta t_4) \\ 0 \\ 0 \end{bmatrix}, \quad \begin{bmatrix} \bar{\theta}(1) \\ \bar{\omega}(1) \\ \dot{\bar{\omega}}(1) \end{bmatrix} = \begin{bmatrix} \theta_f \\ 0 \\ 0 \end{bmatrix}, \tag{14}$$

$$\begin{aligned} a &= \bar{\theta}(0), \\ b &= \bar{\omega}(0), \\ c &= \frac{1}{2}\dot{\bar{\omega}}(0), \\ d &= 0, \\ e &= 0. \end{aligned} \tag{15}$$

Also, the coefficients f, g, and h can be easily computed by Equation (16), and $\theta(t)$, $\omega(t)$, and $\dot{\omega}(t)$ for the exit phase can be defined by Equation (7).

$$\begin{bmatrix} 1 & 1 & 1 \\ 5 & 6 & 7 \\ 20 & 30 & 42 \end{bmatrix} \begin{bmatrix} f \\ g \\ h \end{bmatrix} = \begin{bmatrix} \bar{\theta}(1) - (a+b+c) \\ \bar{\omega}(1) - (b+2c) \\ \bar{\omega}'(1) - (2c) \end{bmatrix}. \tag{16}$$

Table 3: Parameter description for Figure 3.

θ^i_{t5}	Final value of the exit phase
t_5	Final time of the exit phase
i	Iteration number
θ_f	Boundary condition at final time
G	Gradient of error
γ	Tuning parameter for G
Δ	Perturbation value for $\dot{\omega}_{max}$
ε	Tolerance of error

Table 4: Boundary conditions for attitude trajectory [18].

$t_0 = 0.0$ (s)	$t_f = 5.0$ s
$\theta_0 = 0.0$ (deg)	$\theta_f = 180.0$ deg
$\omega_0 = 0.0$ (deg/s)	$\omega_f = 0.0$ deg/s
$\dot{\omega}_0 = 0.0$ (deg/s^2)	$\dot{\omega}_f = 0.0$ deg/s^2
$\ddot{\omega}_0 = 0.0$ (deg/s^3)	$\ddot{\omega}_f = 0.0$ deg/s^3
$\dddot{\omega}_0 = 0.0$ (deg/s^4)	$\dddot{\omega}_f = 0.0$ deg/s^4

Then, we should find the $\dot{\omega}_{max}$ to create the trajectories $\theta(t)$, $\omega(t)$, and $\dot{\omega}(t)$ satisfying the boundary conditions in the given time interval. If $\dot{\omega}_{max}$ is not the optimal value, the trajectory satisfying the boundary conditions cannot be generated. We use the Newton-Raphson method to calculate the $\dot{\omega}_{max}$ satisfying the boundary conditions to avoid this problem.

3.6. Calculation of the Maximum Acceleration. Figure 3 is the Newton-Raphson method to compute $\dot{\omega}_{max}$. The algorithm

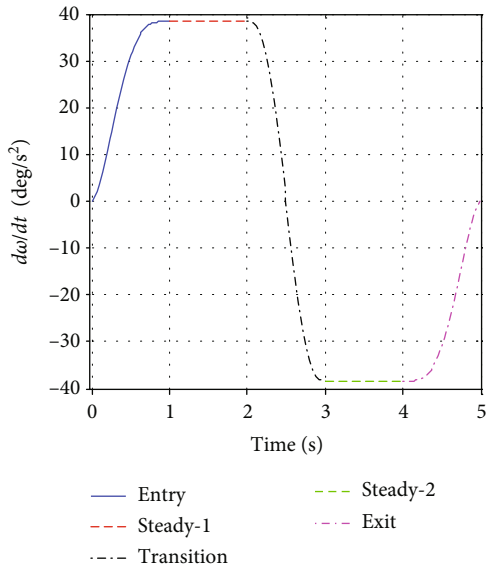

Figure 4: Trajectory of acceleration of attitude.

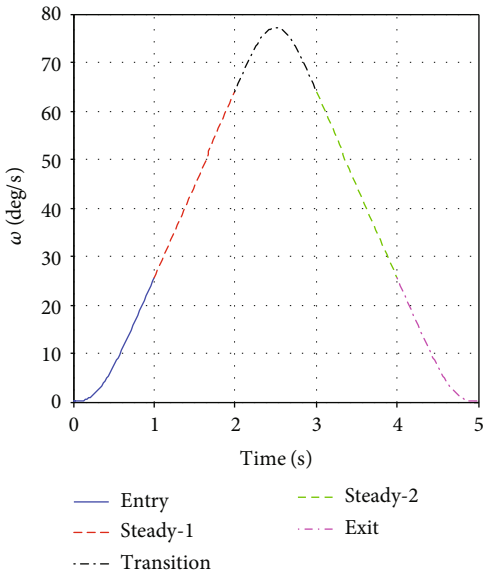

Figure 5: Trajectory of angular rate of attitude.

as shown in Figure 3 is divided into two sections. The sections are distinguished as a green box and a blue box. The section expressed by the green box indicates the procedure of calculating the initial $\dot{\omega}_{\max}$, whereas the section written by the blue box shows the procedure of iterative calculation of $\dot{\omega}_{\max}$ satisfying the boundary conditions. The parameters in Figure 3 are described in Table 3.

Briefly describing Figure 3, the initial trajectory is generated after defining the boundary conditions in the section of the green box. Then, the trajectory is reproduced by $\dot{\omega}_{\max_0} + \Delta$ in the section of the blue box. The regenerated trajectory is used as the initial trajectory for iterative computation. The error e_{i+1} between the final value $\theta_{t_5}^{i+1}$ of the regenerated trajectory and the boundary conditions θ_f at the final time is computed. The error e_{i+1} is computed for each calculation. Next, the error gradient G is calculated, which is used to update $\dot{\omega}_{\max}$. Finally, the tolerance check is implemented. If the error tolerance is satisfied, the computation algorithm

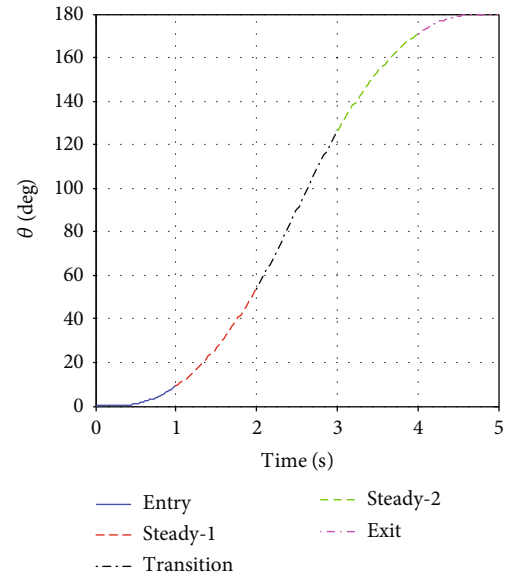

Figure 6: Trajectory of attitude angle satisfying boundary conditions.

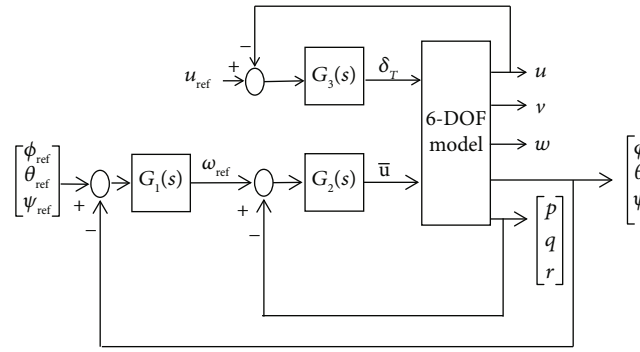

Figure 7: Block diagram of the ACAH system and SCSH system.

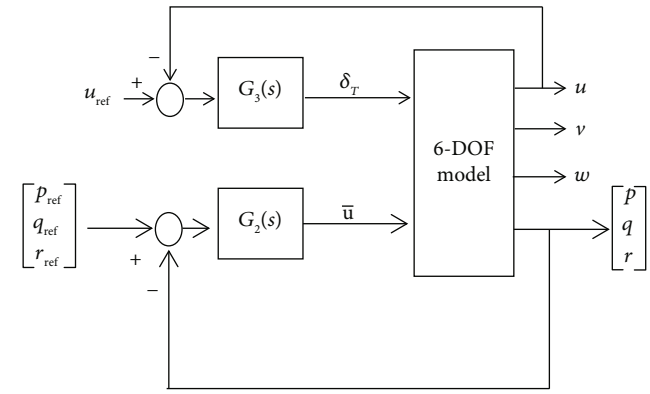

Figure 8: Block diagram of the RCRH system and SCSH system.

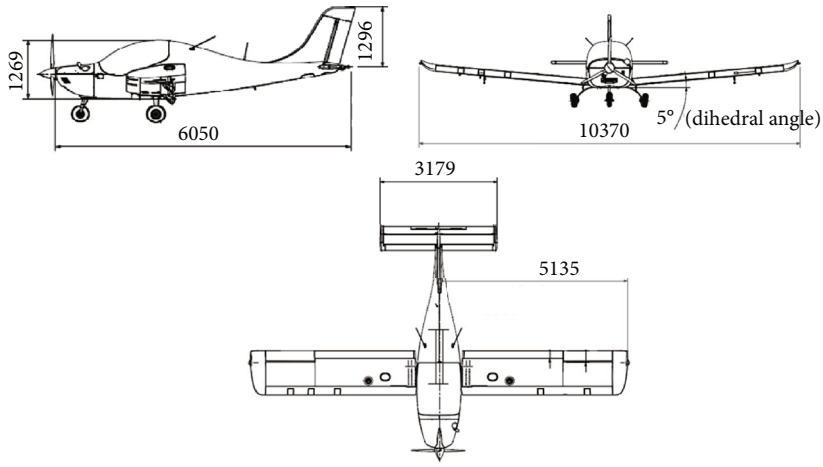

Figure 9: Shape of KLA-100 aircraft (unit: mm).

of $\dot{\omega}_{\max}$ is terminated. The attitude trajectory is produced after specifying the boundary condition as shown in Table 4 in order to check whether the trajectory can be generated by the proposed method or not.

Figures 4–6 indicate the generated trajectories $\theta(t)$, $\omega(t)$, and $\dot{\omega}(t)$ by using polynomials and the Newton-Raphson method. The maximum acceleration $\dot{\omega}_{\max}$ has been calculated as 38 (deg/s^2). So, the boundary conditions defined by Table 4 have been satisfied, and the trajectory $\theta(t)$ associated with modal inputs is computed, which is physically reasonable. Therefore, the proposed method with 7$^{\text{th}}$-order polynomials and the Newton-Raphson method to generate the maneuver libraries are feasible.

4. Design of the Control law

This section deals with the design of the control laws for tactical maneuvers. The ACAH system, RCRH system, and SCSH system are designed with the PID control technique. The reason why the PID control technique has been used is that we want to check the usefulness of the control system using maneuver libraries. If the control system using maneuver libraries with the PID control technique can successfully implement the tactical maneuvers, the aggressive maneuvers of fixed-wing aircraft can be performed without a complex algorithm of the flight path generation, guidance, and control technique, which can guarantee real-time flight control. Furthermore, the weight and the volume of the payloads can be reduced. Figures 7 and 8 are the structure of the ACAH system and RCRH system with the SCSH system, respectively. The detailed information for designing the ACAH system, RCRH system, and SCSH system using the PID control technique can be found in Refs. [19–22]. These FCSs are allocated to each maneuver library as shown in Table 2. So, the control systems have to be switched when the maneuver libraries change.

In Figures 7 and 8, u_{ref} is the forward speed command and ω_{ref} is the angular rate command $[p_{\text{ref}}\ q_{\text{ref}}\ r_{\text{ref}}]^T$. $\bar{\mathbf{u}}$ is the control deflection angle $[\delta_a\ \delta_e\ \delta_r]^T$. The control deflection angles mean the deflections of the aileron, elevator, and rudder. $G_1(s)$, $G_2(s)$, and $G_3(s)$ are the PID controller. 6 DOF (degree of freedom) is the flight dynamics model. Figure 9 indicates the shape of a KLA-100 sports light aircraft. The configuration data of the KLA-100 has been defined in Table 5.

Table 5: Configuration data of KLA-100 aircraft.

Maximum weight	620 kg
Maximum engine power	100 hp
Propeller diameter	1,700 mm
Propeller pitch angle at 0.75R	28.527 deg
Main wing span	10.311 m
Main wing reference area	11.607 m^2

5. Application

The two type of maneuvers which are the longitudinal loop and the Immelmann-turn are performed to check the applicability of the proposed FCS using maneuver libraries.

5.1. Longitudinal Loop Maneuver. The longitudinal loop is a maneuver rotating 360 deg around the pitch axis. The procedures for implementing the longitudinal loop maneuver can be found in Ref. [23]. Table 6 is the combination of maneuver libraries for the longitudinal loop. The maximum flight speed of the KLA-100 aircraft has been defined as 240 km/h. However, the maximum speed is limited by aircraft flight instruction because the maximum speed can damage the engine such as engine failure. Therefore, the flight speed for simulation is defined as 200 km/h to avoid engine failure.

The modal inputs for a level flight in Table 6 follow the trim value calculated at 200 km/h. To implement the longitudinal loop, the value of $\dot{\theta}$ has to be determined because the radius of the longitudinal loop is calculated by $\dot{\theta}$. The relation between $\dot{\theta}$ and the radius of the longitudinal loop is defined as $r_{\text{loop}} = V_T/\dot{\theta}$ [2]. The analysis results are illustrated in Figure 10. It is judged that a faster rotation speed than

Table 6: Longitudinal loop maneuver.

	Maneuver	Modal input	Time interval (s)	Controller
q_0	Level flight	$V_T = 200.0$ (km/h) $\alpha = 0.8422$ (deg)	[0.0 2.0]	(i) ACAH system (ii) SCSH system
q_3	Longitudinal loop	$V_T = 200.0$ (km/h) $\dot{\theta} = 40.0$ (deg/s) $r_{\text{loop}} = 70.0$ (m)	[2.0 11.3]	(i) RCRH system (ii) SCSH system
q_0	Level flight	$V_T = 200.0$ (km/h) $\alpha = 0.8422$ (deg)	[11.3 21.5]	(i) ACAH system (ii) SCSH system

40 deg/s cannot be maintained during the maneuver, whereas a slower rotation speed than 40 deg/s cannot be used for the longitudinal loop because the radius of the loop maneuver is so high. Thus, Figure 10 shows that the 40 deg/s is the appropriate angular rate for $\dot{\theta}$. So, the best radius of the longitudinal loop is 70 m. The analysis result is applied to Table 6.

Figure 11 displays the simulation results of the longitudinal loop. Figures 11(a) and 11(b) illustrate the flight path and velocity for the longitudinal loop, respectively. Figure 11(b) shows that the vertical velocity w is dramatically increased during the longitudinal loop maneuver. This means that the longitudinal loop maneuver is a high angle of attack (AOA) operation. Figure 11(c) indicates the trajectory of the angular rates during the maneuver. The pitch rate q has been maintained around 40 deg/s. The roll rate p and yaw rate r are maintained around 0 deg/s. The 40 deg/s and 0 deg/s are used as command signals for FCS. So, the RCRH system using the PID control technique is properly designed, and the longitudinal loop maneuver can be performed without the nonlinear control technique. Figure 11(d) is the simulated trajectory of the attitude angle. The roll angle ϕ is suddenly changed by about 5 s, which means the aircraft performs the upside-down flight. The roll angle is recovered to 0 deg to implement the level flight after finishing the loop maneuver. The variation of pitch and directional angles is physically correct to complete the longitudinal loop maneuver. Therefore, the longitudinal loop maneuver can be successfully performed by the proposed FCS using maneuver libraries.

5.2. Immelmann-Turn Maneuver. The Immelmann-turn maneuver is a highly aggressive maneuver to reverse the flight direction. The maneuver is constructed by a level flight, half-loop, and roll maneuver. The Immelmann-turn maneuver is finished when the aircraft direction is changed to opposite with the level flight. The flight simulation for the Immelmann turn is implemented by a combination of maneuver libraries like in Table 7. In particular, $\dot{\phi}$ is used as the modal input for the roll maneuver, and it is defined as 60 deg/s to change the roll angle from 180 deg to 0 deg.

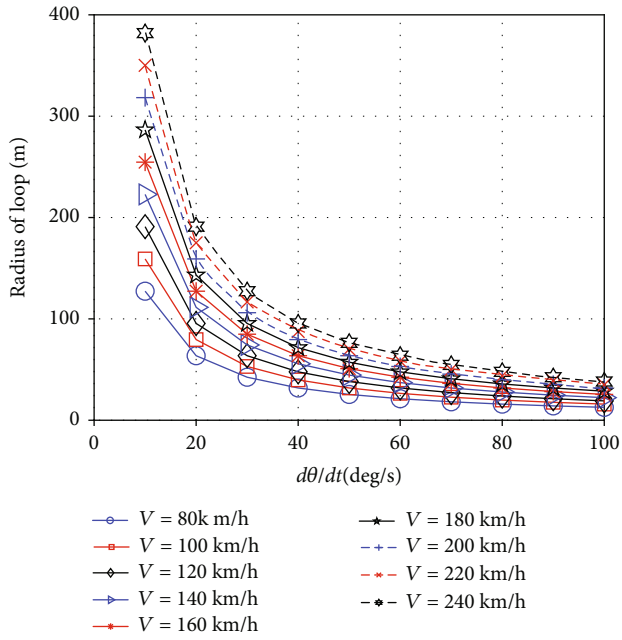

Figure 10: The radius of the loop maneuver versus the rotation speed [18].

Figures 12(a) and 12(b) represent the flight path and variation of flight velocity for the Immelmann turn, respectively. In Figure 12(b), the vertical velocity w is extremely raised while performing a half-loop maneuver. The characteristic of the loop maneuver has already been mentioned in Figure 11. The lateral velocity v is extremely increased while implementing the roll maneuver, which highly raises the side force. Here, v is increased to approximately -13 m/s, which means the maneuver library to cancel the side force has to be defined. In Figure 12(c), the pitch rate q is maintained around 40 deg/s during the half-loop maneuver while maintaining the roll and directional rates as 60 deg/s and 0 deg/s, respectively. So, it is judged that FCS has been well operated and designed to perform the Immelmann-turn maneuver. Figure 12(d) illustrates the variation of attitude angles. The attitude angles are changed as expected, which are physically reasonable. Consequently, the Immelmann-turn maneuver

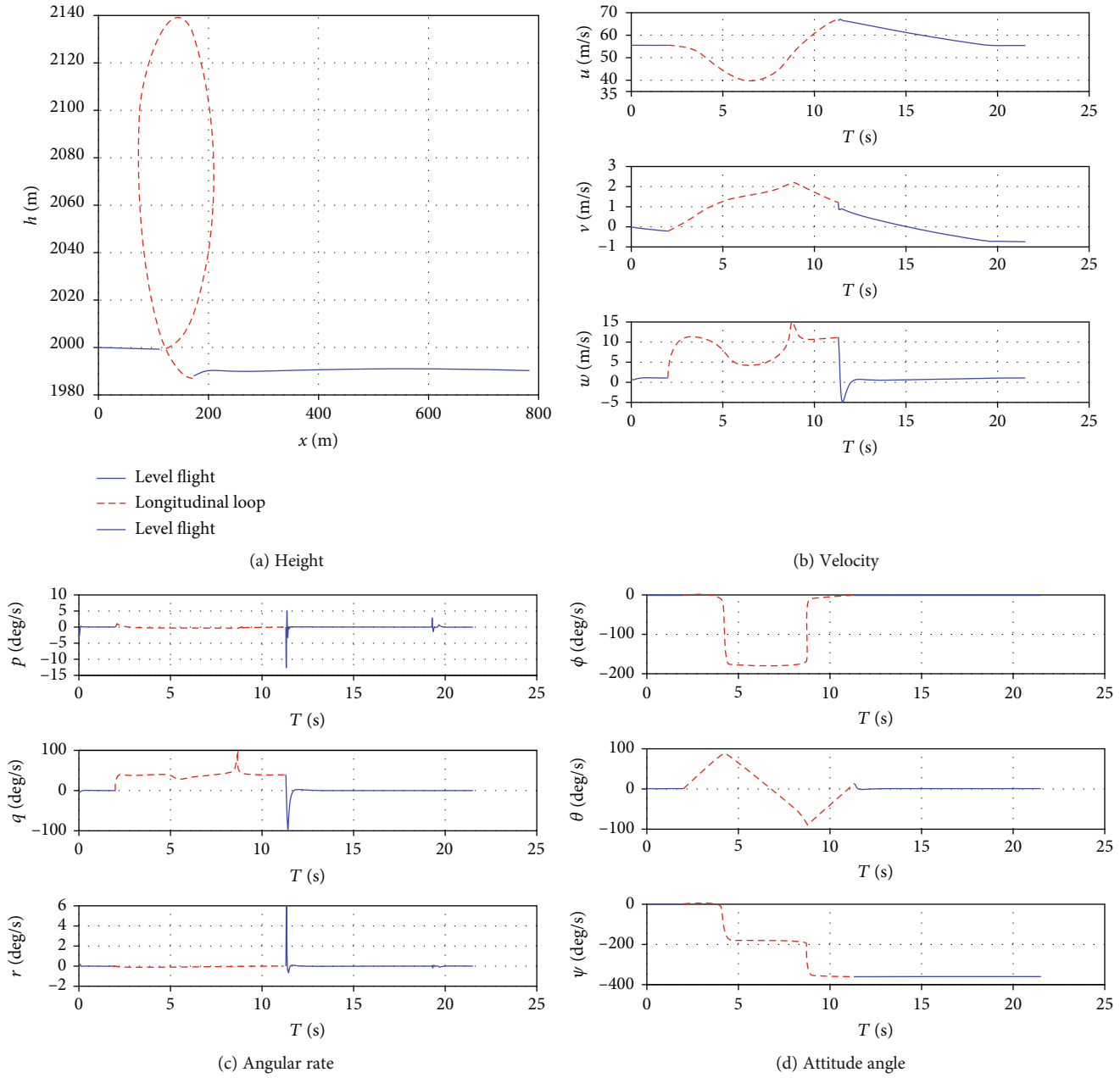

Figure 11: Flight simulation results of longitudinal loop maneuver.

can be successfully implemented by the proposed FCS using maneuver libraries.

6. Conclusion

The real-time maneuver library generation technique and the FCS using general maneuver libraries have been suggested and validated in this research. The required tactical maneuvers to implement the typical air-to-ground mission can be constructed by combination of maneuver libraries. Each maneuver libraries to implement the tactical maneuvers can be defined by the several modal inputs and the FCS using the PID control technique. Thus, the generation of maneuver libraries is the same with creating the trajectory of modal inputs. Here, each maneuver library is generated by a 7^{th}-order polynomial. The FCS are designed for three types of control systems such as the ACAH system, RCRH system, and SCSH system, which satisfy the aggressiveness of tactical maneuvers. Finally, the series of flight simulations have been implemented for longitudinal loop and Immelmann-turn maneuver to examine the effect of the suggested FCS.

The longitudinal loop maneuver is built by three maneuver libraries that are the level, loop, and level flight. The ACAH system, RCRH system, and SCSH system track well the trajectory of modal inputs. The flight simulation results show that the longitudinal loop maneuver can be successfully implemented by maneuver libraries with FCS using the PID

Table 7: Immelmann-turn maneuver.

	Maneuver	Modal input	Time interval (s)	Controller
q_0	Level	$V_T = 200.0$ (km/h) $\alpha = 0.8422$ (deg)	[0.0 2.0]	(i) ACAH system (ii) SCSH system
q_3	Longitudinal loop	$V_T = 200.0$ (km/h) $\dot{\theta} = 40.0$ (deg/s) $r_{\text{loop}} = 70.0$ (m)	[2.0 7.0]	(i) RCRH system (ii) SCSH system
q_0	Level	$V_T = 200.0$ (km/h) $\alpha = 0.8422$ (deg)	[7.0 9.0]	(i) ACAH system (ii) SCSH system
q_2	Roll	$V_T = 200.0$ (km/h) $\dot{\phi} = 60.0$ (deg/s)	[9.0 12.0]	(i) RCRH system (ii) SCSH system
q_0	Level	$V_T = 200.0$ (km/h) $\alpha = 0.8422$ (deg)	[12.0 14.8]	(i) ACAH system (ii) SCSH system

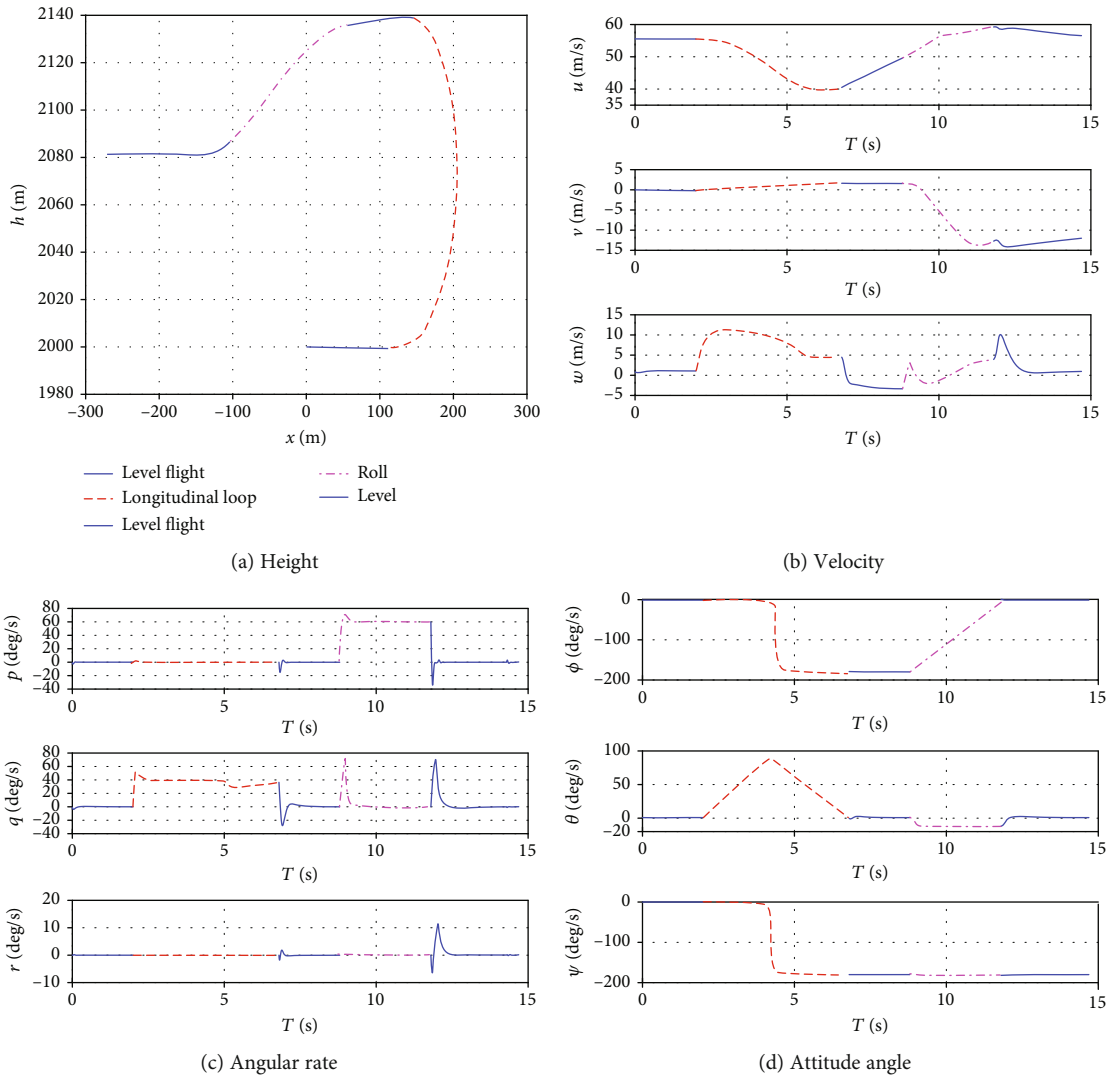

(a) Height

(b) Velocity

(c) Angular rate

(d) Attitude angle

Figure 12: Flight simulation results of the Immelmann-turn maneuver.

control technique. The Immelmann-turn maneuver additionally includes the 180 deg roll maneuver. The RCRH system is the main controller to perform the half-loop and the roll maneuver. So, the RCRH system is the key control system that leads the completion of the Immelmann-turn maneuver.

Typically, these two maneuvers are the key tactical maneuvers in battlefields. All tactical maneuvers can be performed by the suggested techniques, and new tactical maneuvers for fixed-wing aircraft, rotorcraft, and compound aircraft can be developed by the proposed techniques. Moreover, the tactical maneuvers can be implemented in real time. Therefore, it is judged that all of the tactical maneuvers were significantly performed by the proposed maneuver libraries and FCS, which can contribute to developing micro aircraft and enhance the survivability of manned and unmanned aircraft in complicated battlefields.

Data Availability

(1) The Table 2 data used to support the finding of this study have been deposited in the Nazmi JU. (2) The Figure 2 data used to support the finding of this study have been deposited in the Douglas Tomson repository. (3) The Figure 9 and Table 5 data used to support the finding of this study have been deposited in the Lee DH repository. (4) The data used to support the finding of this study are available from the first and corresponding authors upon request.

Conflicts of Interest

The authors declare that there is no conflict of interest regarding the publication of this paper.

Funding

This work was conducted at the High-Speed Compound Unmanned Rotorcraft (HCUR) research laboratory with the support of the Agency for Defense Development (ADD).

References

[1] Z. Yu, C. Jing, and L. Shen, "Real-time trajectory planning for UCAV air-to-surface attack using inverse dynamics optimization method and receding horizon control," *Chinese Journal of Aeronautics*, vol. 26, no. 4, pp. 1038–1056, 2013.

[2] N. K. Ure and G. Inalhan, "Design of a multi modal control framework for agile maneuvering UCAV," in *2009 IEEE Aerospace conference*, pp. 1–10, IEEE, Big Sky, MT, USA, March 2009.

[3] J. U. Nazim and I. Gokhan, "Design of higher order sliding mode control laws for agile maneuvering UCAV," in *2nd international symposium on systems and control in aerospace and astronautics*, 2008.

[4] T. J. Koo, G. J. Pappas, and S. Sebastian, "Multi-modal control of systems with constraints," in *Proceedings of the 40th IEEE Conference on Decision and Control (Cat. No.01CH37228)*, pp. 2075–2080, Orlando, FL, USA, USA, 2001.

[5] Y. J. Wang, J. Dong, X. Liu, and L. Zhang, "Identification and standardization of maneuvers based upon operational flight data," *Chinese Journal of Aeronautics*, vol. 28, no. 1, pp. 133–140, 2015.

[6] S. Arora, S. Choudhury, D. Althoff, and S. Scherer, "Emergency maneuver library-ensuring safe navigation in partially known environments," in *2015 IEEE international conference on robotics and automation (ICRA)*, pp. 6431–6438, IEEE, Seattle, WA, USA, 2015.

[7] A. Bry, C. Richter, A. Bachrach, and N. Roy, "Aggressive flight of fixed-wing and quadrotor aircraft in dense indoor environments," *The International Journal of Robotics Research*, vol. 34, no. 7, pp. 969–1002, 2015.

[8] A. J. Barry, P. R. Florence, and R. Tedrake, "High-speed autonomous obstacle avoidance with pushbroom stereo," *Journal of Field Robotics*, vol. 35, no. 1, pp. 52–68, 2018.

[9] C. R. Brian, *Control System Development for Autonomous Aerobatic Maneuvering with a Fixed-Wing Aircraft*, Auburn University, 2014.

[10] J. H. Willem, *Autonomous Aerobatic Flight of a Fixed Wing Unmanned Aerial Vehicle*, Stellenbosch University, 2007.

[11] A. F. B. C. A. Edwards, *Chapter 6 maneuvering flight*, USA test pilot school, 1990, Report No. 19970117 033.

[12] M. B. Tatsch, *Flight training instruction*, Naval Air Training Command, 2014, Report No. CNATRA P-764 (08-14) PAT.

[13] H. van der Plas and H. G. Visser, "Trajectory optimisation of an aerobatic air race," *The Aeronautical Journal*, vol. 113, no. 1139, pp. 1–8, 2009.

[14] D. G. Thomson and R. Bradley, "Mathematical definition of helicopter maneuvers," *Journal of the American Helicopter Society*, vol. 42, no. 4, pp. 307–309, 1997.

[15] D. H. Lee, S. W. Hur, S. H. Lee, S. H. Kang, and C. J. Kim, "Flight path generation using polynomial and trajectory tracking control for the small aircraft," in *Proc. of 2011 fall meeting of the korea society aeronautical and space science*, pp. 219-220, 2017.

[16] D. H. Lee, C. J. Kim, S. W. Hur, and S. H. Lee, "A study on the flight path generation using polynomials and tracking control," *Journal of Institute of Control, Robotics and Systems*, vol. 24, no. 11, pp. 1059–1068, 2018.

[17] Department of Defense, *Flying qualities of piloted aircraft*, Department of Defense, Seoul, 1997.

[18] D. H. Lee, C.-J. Kim, S. W. Hur, and S. H. Lee, "Implementation of tactical maneuvers with maneuver libraries," *Chinese Journal of Aeronautics*, 2019.

[19] O. Katsuhiko, *Modern Control Engineering 5th Edition*, Pearson Education, Korea, Seoul, 2010.

[20] H. B. John, *Automatic Control of Aircraft and Missiles 2nd Edition*, A wiley-Interscience Publication, New Jersey, 1991.

[21] J. H. Blakelock, *Automatic Control of Aircraft and Missiles, Second Edition*, A Wiley-interscience Publication, 1991.

[22] P. Poksawat, *Control system for fixed-wing unmanned aerial vehicles: automatic tuning, gain scheduling, and turbulence mitigation*, RMIT University, 2018.

[23] H. Takano and Y. Baba, "Optimal flight trajectory and aerobatic maneuvers against missiles," in *2004 5th Asian control conference*, pp. 1841–1848, 2004.

[24] Department of Defense, *Flying qualities of piloted airplanes*, Department of Defense, Seoul, 1980.